SENRA Academic Publishers, Burnaby, British Columbia
Vol. 3, No. 3, pp. 903-910, 2009
ISSN: 1715-9997

Canadian Journal of pure&applied sciences

THE INFLUENCE OF MONO-DISPERSED TIN – DOPED INDIUM OXIDE NANOPOWDERS ON ITS DIELECTRIC PROPERTIES

FF Hammad[1] and *AH Salama[2]
[1]Department of Inorganic Chemistry, National Research Center, Dokki, Giza
[2]Department Physical Chemistry, National Research Center, Dokki, Giza

ABSTRACT

Mono-dispersed tin doped indium oxide (ITO) nanopowders were prepared by wet chemical co-precipitation method at 300^0C for 3h with maintaining the In/Sn atomic ratio 90:10, 70:30 and 50: 50 wt.%. The grain size of the prepared samples was determined by TEM technique. Structural characterization of the prepared samples was studied by X-ray diffraction analysis. It is found that the samples were a mixture of cubic and rhombohedra crystals with sharp diffraction peaks except for the sample with atomic ratio 50:50 shows very poor crystalline and no peaks ascribed to the phase of the compounds are observed which confirms the amorphicity of this sample. The dielectric properties including dielectric constant, έ and dielectric loss, ε`` of the prepared samples were evaluated from the observed capacitance values in the frequency range 100 Hz to 5 MHz and in the temperature range of 25 ^{0}C to 160^0C. Further, from the dielectric properties studies AC- conductivity was evaluated. The activation enthalpy ΔH and the entropy change ΔS of the prepared samples were calculated. The obtained data were correlated to the structure of the prepared samples.

Keywords: Indium Tin Oxide nanopowder, XRD- spectroscopy, dielectric constant έ, dielectric loss ε``, ac-conductivity.

INTRODUCTION

Indium tin oxide is a colorless in thin layers solid solution of In_2O_3 and SnO_2 (typically 90% In_2O_3 and 10% SnO_2 by weight). In_2O_3 is an important transparent conducting oxide (TCO) material, passing over 90% of visible light. Increased interest to In_2O_3, which is one of the wide band gap semi conducting materials (3.6 or ~3.7eV) (Korotcenkov, *et al*., 2007; Zhu *et al*., 2005; Rey *et al*., 2005) and crystallizes with C-type rare earth sesquioxide structure. Due to the wide band gap, it is transparent to the visible radiation. It is an insulator in its stoichiometric form and becomes conducting in the oxygen deficient nonstoichiometric form. Each oxygen vacancy can act like a doubly or singly ionized donor. Therefore, nonstoichiometric In_2O_3 exhibits high electrical conductivity similar to that of a heavily doped degenerate n-type semiconductor (Malar *et al*., 2005; Zhan *et al*., 2004). The interest in nonstoichiometric In_2O_3 is mainly due to the possibility of varying the electrical resistivity by more than 10 orders of magnitude by changing the oxygen content alone (Malar *et al*., 2005).

Indium tin oxide (ITO) is an advanced ceramic material with many electronic and optical applications due to its excellent properties of high conductivity ($\approx 10^4$ $\Omega^{-1}cm^{-1}$) and high transparency (85-90%) to visible light, high infrared reflectivity for wavelengths higher than 1 μm (Lee and Choi, 2005).

Up till now, tin-doped indium oxide (ITO) yields the lowest resistivity of about 1.10^{-4} Ω cm. This, together with its very good stability, are the reasons why ITO is presently used exclusively as transparent electrode material for flat panel displays, based on liquid crystals, micro plasmas or organic light emitting diodes (OLED) and sensors (Ellmer and Mientus, 2008). High conductivity of ITO is achieved by doping with Sn and thereby increasing the oxygen vacancies in the In_2O_3 lattice. An improvement of conductivity can also be achieved by stabilizing the cubic In_2O_3 phase instead of the hexagonal modification (Pujilaksono *et al*., 2005).

To increase the conductivity up to the metallic conductivity (10^3-10^4 $\Omega^{-1}cm^{-1}$), a solid solution of indium-tin oxide (ITO) with a few percent of Sn is used (Cho *et al*., 2006).

ITO thin films of nanoparticles have been reported by Sung *et al*., 1996. In recent years, great attention has been paid to nanometresized materials in studies of their fundamental mechanism, such as the size effect and the quantum effect, and in applications of these materials. In particular, nanocrystalline indium-doped tin dioxide powders are widely applied by a screen-printing technique (Yang *et al*., 1998).

The present work aims to study the effect of different additives ratio of Sn on the crystallographic structure properties and dielectric properties of In_2O_3 using X-ray diffraction analysis, dielectric constant ε`, dielectric loss ε`` and ac- conductivity in order to select the best composition of In / Sn having cubic structure with higher dielectric properties.

*Corresponding author email: alia2005salama@yahoo.com

MATERIALS AND METHODS

Preparation of nano-grain ITO

Indium tin oxide (ITO) nano powders of different compositions (In: Sn = 90: 10, 70: 30 and 50: 50 wt.%) were prepared from the starting materials, aqueous indium nitrate and $SnCl_4.5H_2O$. The resulting solution was stirred genetically for 2h at 65^oC and the pH of the above solution was maintained in the range 7.0-7.5. White powder solid was obtained. The samples were heated at 300 ^oC at 3h (Jagadish *et al*., 2003).

TEM

TEM images were taken with a JEDL model 1230 Transimation Electron Microscope.

X-ray diffraction study

A computer controlled X-ray diffraction (Diano- 8000, USA) was used with a filtered Co K_α radiation (λ= 1.7903$\mathring{}$A). The scanning range was 20$\mathring{}$ -80$\mathring{}$ (2θ).

Dielectric properties

The dielectric properties (dielectric constant $\varepsilon`$ and dielectric loss $\varepsilon``$) were measured as disc of 12 mm diameter, in the temperature range (298 K – 483 K) and frequency range (0.1KHz – 5 MHz) using HIOKI 3532 LCR Hi – Tester.

RESULTS AND DISCUSSION

TEM

Figure 1, shows TEM images of pure In_2O_3 and ITO nanopowder of different compositions namely (90: 10, 70: 30 and 50: 50 wt.%). It is clear that the particle was in spherical shape with size range from 10 nm to 70 nm.

X-ray diffraction for ITO nanopowder

Figure 2a and 2b, Shows XRD patterns of pure In_2O_3 and indium tin oxide (ITO) nanopowder of different composition namely (In: Sn = 90:10, 70:30 and 50:50 wt.%). It is clear that there is no any diffraction line for separate In_2O_3 or SnO_2. It is found that the samples were a mixture of cubic and rhombohedra In_2O_3 and SnO_2 with sharp diffraction peaks. The deconvoluted X-ray peaks of (222) and (104) corresponding to cubic and rhombohedra In_2O_3 respectively in confirmed with the result obtained by Kim *et al*. (1999).

Dielectric properties of ITO samples

Variation of dielectric constant $\varepsilon`$ and dielectric loss $\varepsilon``$ of ITO with frequency and temperatures

Figure 3, shows variation of dielectric constant $\varepsilon`$ with frequency at different temperatures for ITO samples containing different Sn^{4+} ion concentrations. The measurement was carried out in the frequency range from 100 Hz to 5 MHz and in the temperature range from room temperature to 160^oC. From this figure, as the frequency increases the following can be noticed:

The dielectric constant ($\varepsilon`$) is the frequency dependent within the range used. It is clear that it decreases with the increase of frequency at lower frequency range. This decrease can be attributed to the dielectric dispersion originated from the lag of the molecules behind the alternations of the applied electric field. At the higher

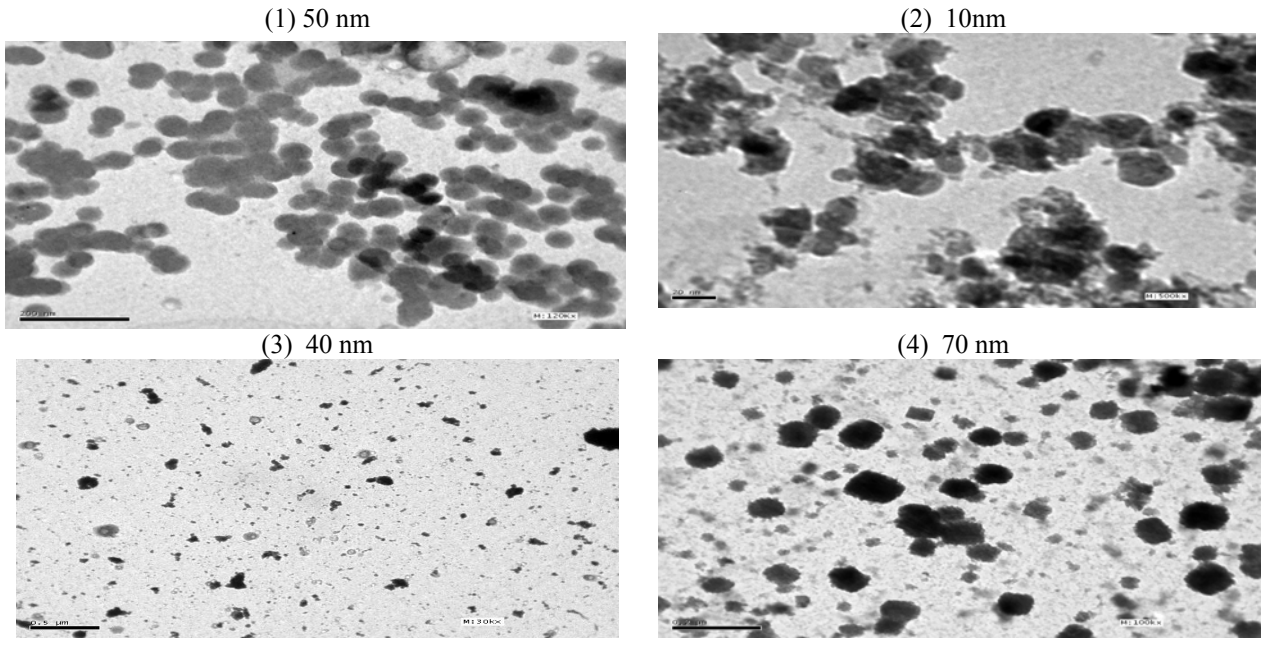

Fig. 1. TEM image of structure ITO particles: (1) Pure In_2O_3, (2) (In: Sn = 90:10), (3) (In: Sn = 70:30) and (4) (In: Sn = 50:50).

frequency range almost at 1 KHz, the dielectric constant becomes frequency independent. This phenomenon can be attributed to the decrease of the apparent carrier mobility. When the ceramic was heated in air, oxygen diffuses into the specimen and this is followed by the formation of a non-conducting oxide layer at the inter-granular spacing. On the oxide layer, space charges easily accumulate to form a high resistance barrier layer for the conduction electrons (Richerson, 1992).

On the other hand, from the measured dielectric loss (ε``) shown in figure 4, increasing frequency is accompanied by a decrease in the dielectric loss with formation of a peak that shifts to higher frequency as the temperature increased. Generally, the values of the dielectric losses varied from 0.9 to 0.1. It can be noticed that, there are

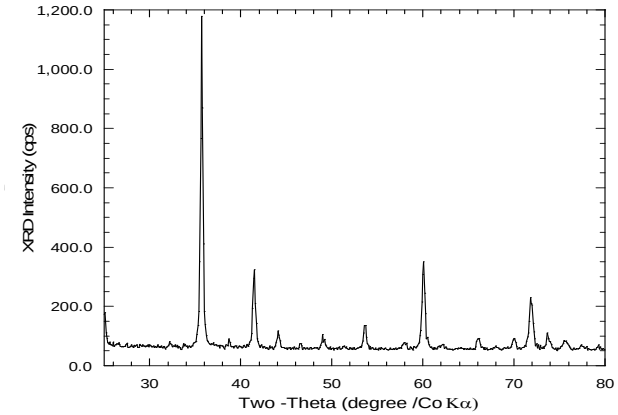

Fig. 2a. X-ray Diffraction pattern for pure In_2O_3.

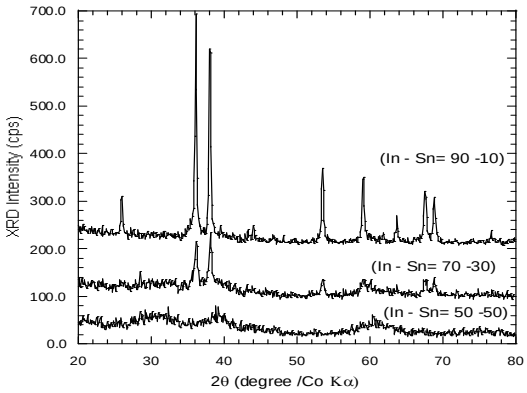

Fig. 2b. X-ray Different Patterns of the samples of different In: Sn ratio heated at 300 ̊C.

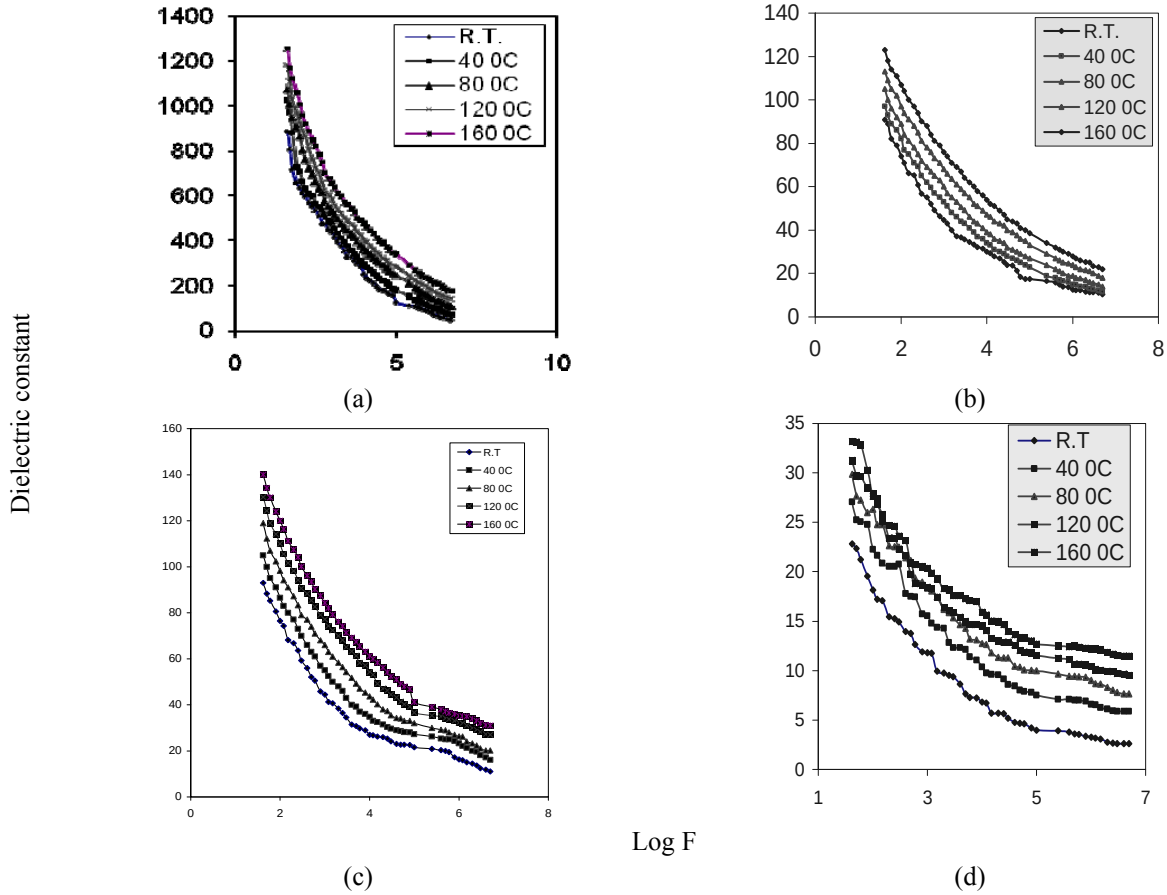

Fig. 3. The frequency dependent of dielectric constant □`a) Pure In_2O_3, (b) (In: Sn = 90:10) , (c) (In: Sn = 70:30) and (d) (In: Sn = 50:50).

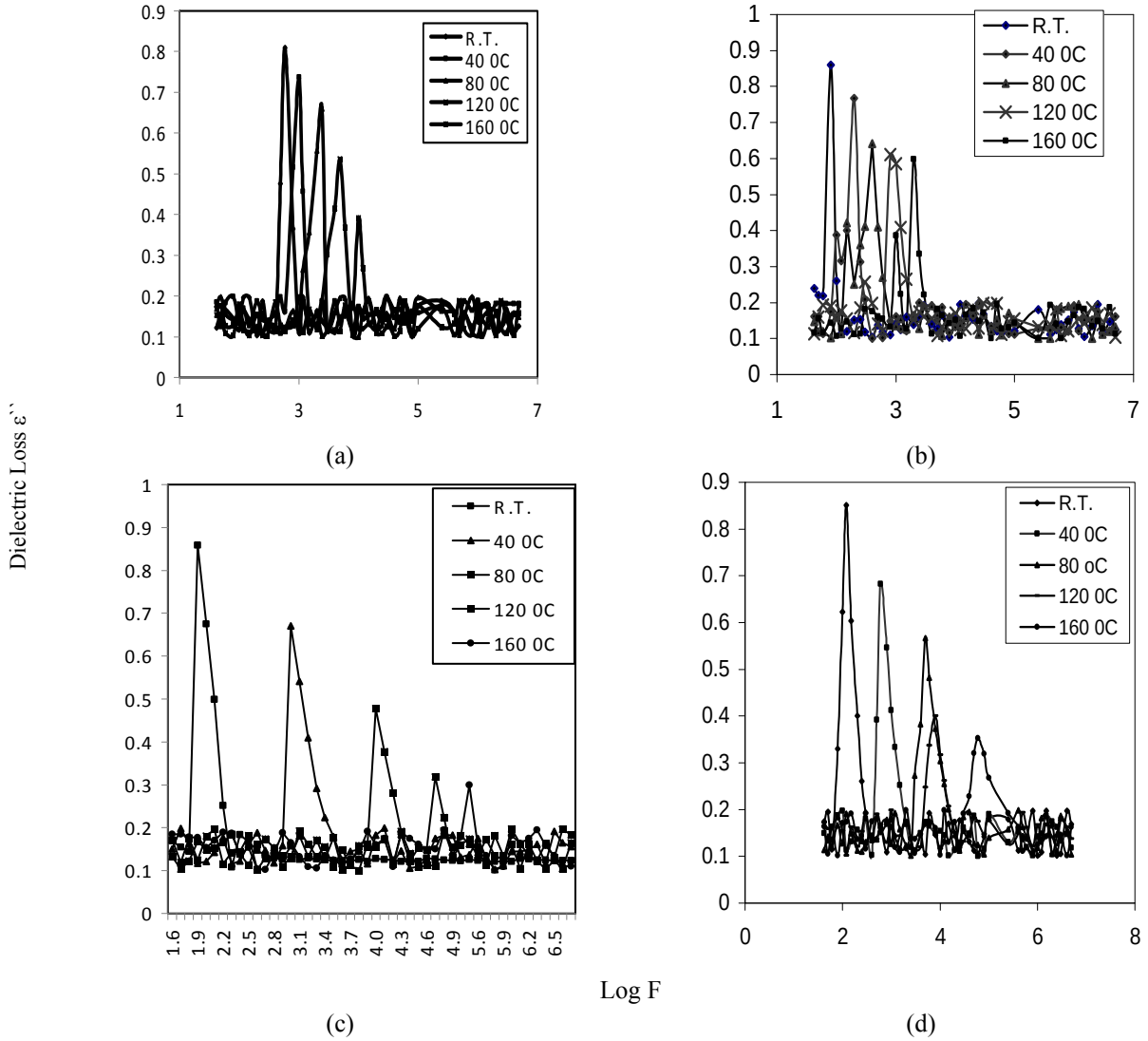

Fig. 4. The frequency dependent of dielectric loss e`` for (a) pure In_2O_3, (b) (In: Sn = 90:10), (c) (In: Sn = 70:30) and (d) (In: Sn = 50:50).

different types of electric energy losses in the presence of alternating electric field. The d.c loss is due to the transitional motion of free charges and it's trapping in holes. The Debye type loss is due to orientation polarization of polar groups, which are able to orient or to polarize in the electric field. The two types of losses are always present, but sometimes one of them is predominant (El-Anwar and El-Sayed, 1997). The loss absorption bands recorded in curves of ε`` vs. log F, show shift towards a higher temperature as the frequency is increased. This shift can be attributed to the increased mobility of free electrons with temperature. The position of F_m, the maxima of the loss absorption bands, for the prepared samples is listed in table 1. The apparent relaxation times for these samples are calculated from the equ.

$$\tau = 1/ 2\pi F_m$$

Where, τ is the apparent relaxation time and F_m is the critical frequency corresponding to maximum energy loss $\varepsilon``_m$. the values obtained are listed in table 1. The activation enthalpy ΔH and the entropy change ΔS of the dielectric relaxation are calculated from the usual rate equation. The calculated values of ΔH and ΔS are also listed in table 1.

The observed low values of activation enthalpy ΔH of the ITO samples with different Sn^{4+} ratio compared to pure In_2O_3, may be attributed to lower orientation polarization as a result of solid nature of the ceramics, which acquires semi-crystalline nature, polarization is partially occur in the molecule through electrons and some ions, that need low activation energy. Otherwise, the entropy change is negative indicating that the rate determining factor is the displacement of the dipoles, which possess a particular

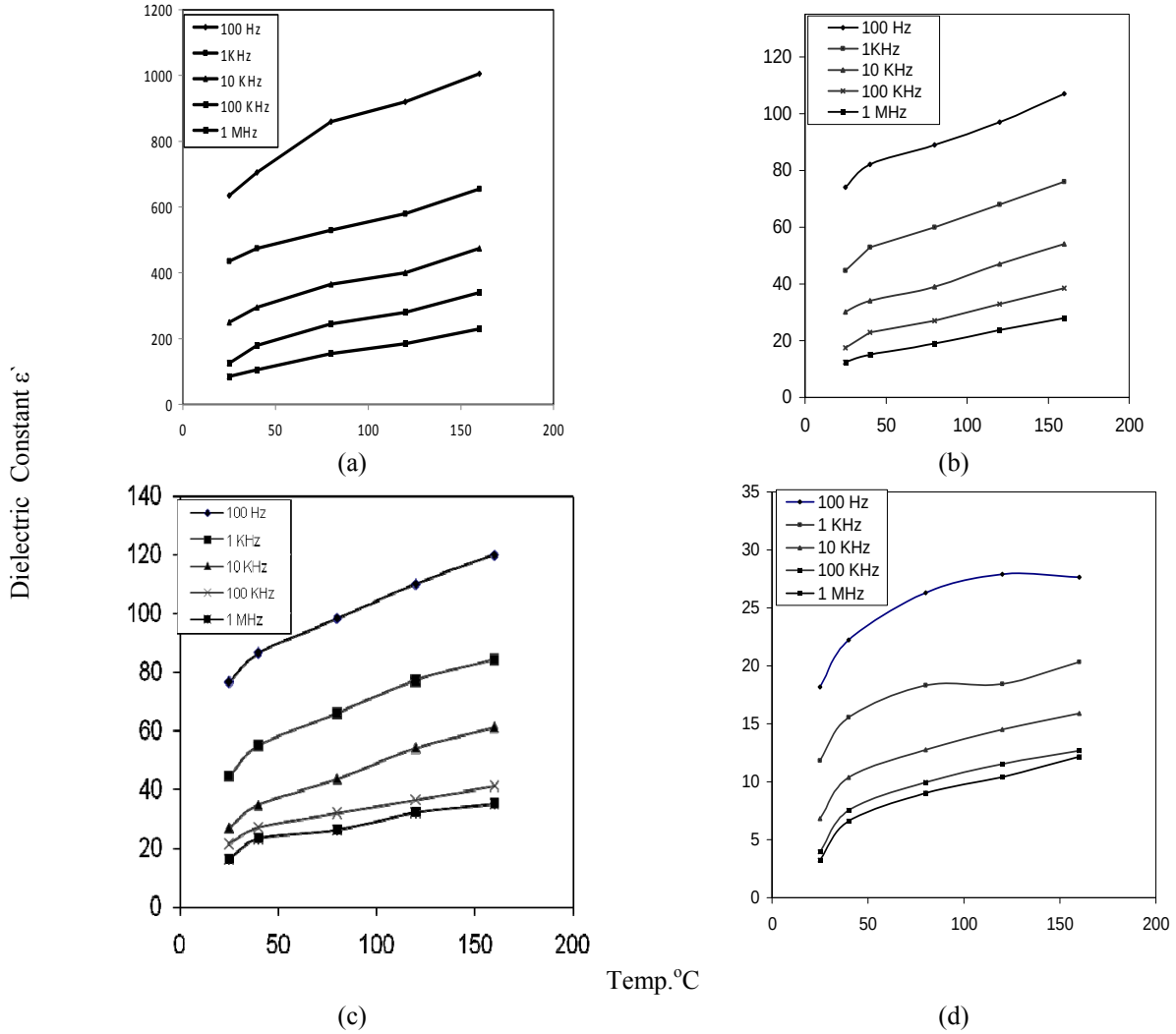

Fig. 5. The variation of dielectric constant as a function of temperature for (a) pure In_2O_3, (b) (In: Sn = 90:10), (c) (In: Sn = 70:30) and (d) (In: Sn = 50:50).

vibration configuration. The negative value of entropy change indicates presence of oscillation polarization and least orientation, i.e., activated molecules is in a state of low order. The relatively stable entropy change values are also indicating that the main chain and the polarization are stables. Accordingly changes that may occur are very low which make these materials good candidates to be used as substrate because of its independent on their constituents.

Figure 6, shows the variation of dielectric constant ε` as a function of $Sn^{4+}$ ion concentration as a doping for $In_2O_3$. The dielectric constant ε` of pure In_2O_3 oxide is very high ranged from 1200 to 100 where as dielectric constant ε` recorded for the ITO samples with different ratio of is very low ranged from 123 to 10.4 for ITO (90:10), from 96 to 10.3 for ITO (70:30) and finally from 33.175 to 2.625 for ITO (50:50). It is clear that as the ratio of Sn^{4+} ion increased the dielectric constant decreased. This behavior may be referred to the fact that, Sn^{4+} with its small ionic radius (0.62 Å) replace In^{3+} ion wits high ionic radius (0.92 Å), leading to shrinkage of the unit cell of the crystal structure. In addition, the very low values of dielectric constant recorded for 50:50 samples may be referred to the amorphicity of this sample and the very grain size of it. The temperature has a strong effect on the crystal structure and polarization characteristics of ITO. Figure 5, shows variation of dielectric constant ε` of ITO samples with different concentrations of $Sn^{4+}$ ion with temperature at different frequencies (100Hz, 1 KHz, 10 KHz, 100 KHz and 1 MHz). The initial increase of ε` can be attributed to the expected decrease in density, which decreases the effect of the environment. Consequently, atomic/ionic polarization tends to increase with temperature.

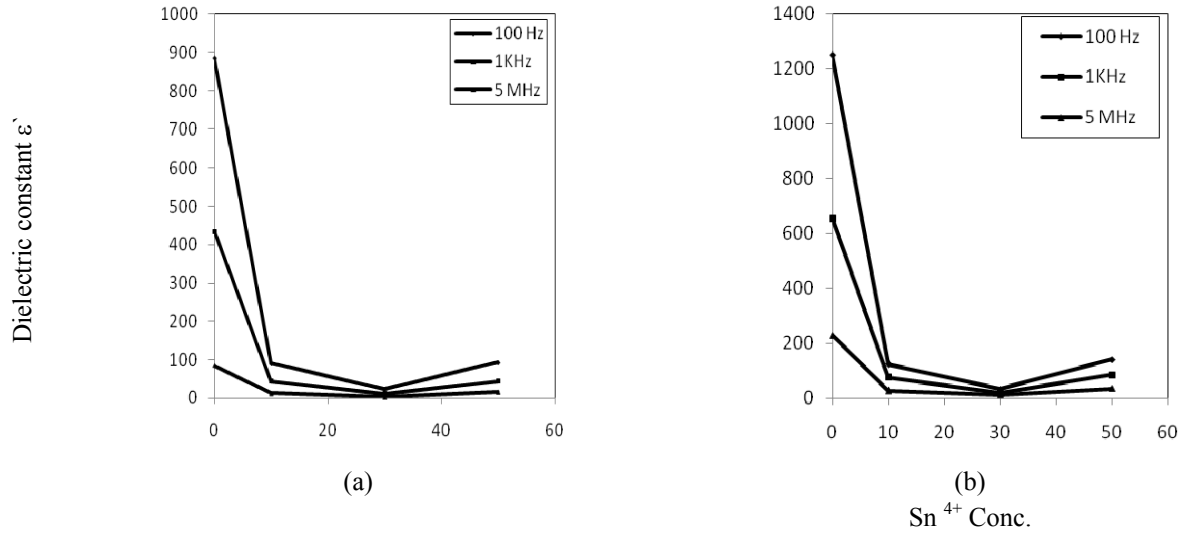

Fig. 6. The variation of dielectric constant ε` with different concentration of Sn $^{+4}$ at (a) room temperature and (b) 160^{o}C .

Table 1. The apparent relaxation time τ (Sec.), the activation enthalpy ΔH and entropy change ΔS for ITO samples with different Sn^{+4} ratio.

Sample	τ(Sec.)					ΔH	ΔS
	R.T	40 ^{0}C	80 ^{0}C	120 ^{0}C	160 ^{0}C	KJ/mole	J/deg/mole
Pure In_2O_3	$2.65x10^{-4}$	$1.59x10^{-4}$	$6.36x10^{-5}$	$3.18x10^{-5}$	$1.59x10^{-5}$	$5.011x10^{3}$	$2.88x10^{-2}$
ITO (90:10)	$1.99x10^{-3}$	$7.96x10^{-4}$	$3.98x10^{-4}$	$1.99x10^{-4}$	$7.96x10^{-5}$	$3.80x10^{-3}$	$-2.817x10^{-2}$
ITO (70:30)	$1.99x10^{-3}$	$1.59x10^{-4}$	$1.59x10^{-5}$	$3.18x10^{-6}$	$6.37x10^{-7}$	$1.48x10^{-3}$	$1.46x10^{-4}$
ITO (50:50)	$1.32x10^{-3}$	$2.65x10^{-4}$	$3.19x10^{-5}$	$1.99x10^{-5}$	$2.65x10^{-6}$	$1.94x10^{-3}$	$4.89x10^{-2}$

Table 2. The data of ac- conductivity for pure In_2O_3 and ITO with different ratio at room temperature and 160^{0}C.

Sample	100 Hz		1KHz		1 MHz	
	Log σ_{ac} (ohm^{-1}cm^{-1})		Log σ_{ac} (ohm^{-1}cm^{-1})		Log σ_{ac} □ (ohm^{-1}cm^{-1})	
	R.T	160 ^{0}C	R.T	160 ^{0}C	R.T	160 ^{0}C
Pure In_2O_3	-9.187	-8.999	-8.214	-7.958	-5.121	-5.040
ITO (90:10)	-9.839	-10.226	-9.103	-8.668	-6.014	-6.037
ITO (70:30)	-8.426	-8.067	-8.059	-7.037	-5.172	-3.995
ITO (50:50)	-7.460	-8.022	-7.002	-7.045	-4.251	-4.162

Moreover, it can be assumed that, the dependence of dielectric constant on the ratio of the Sn^{4+} and consequently on the grain size of the prepared samples figure 6, corresponds to the transfer of water molecules from the surface adsorbed state to the volume adsorbed state under condition of ultra – small pore volume of the nano-sized ITO samples. As ultra-fine volume applies restrictions on evaporation and diffusion.

Variation of ac-conductivity of ITO with frequency

To obtain conductivity (σ_{ac}) due to the dielectric loss ε`` taking 0.9 x 10^{12} as the ratio of the farad to the electrostatic unit of capacitance and of the mho to the electrostatic unit of conductance, and using the expression for the capacitance C_0 in farads of the empty condenser.

$$C_o \frac{A}{4\pi d \times 0.9 \times 10^{12}}$$

The following equation is used,

$$\sigma = \frac{\varepsilon'' \omega}{4\pi d \times 0.9 \times 10^{12}} = \frac{\varepsilon'' F}{1.8 \times 10^{12}} \text{ohm}^{-1}\ \text{cm}^{-1}$$

The dielectric conductivity sums over all dissipation effects and may represent as well as an actual conductivity caused by migrating charge carriers as refer to an energy loss associated with a frequency dependence (dispersion of ε`) for example to the friction accompanying the orientation of the dipoles. The values of ac-conductivity are listed in table 2.

As the measurement was carried out in air, oxygen is absorbed from the environment and since the temperature was raised from room temperature to 160^0C, H_2O molecules were desorbed from the crystal structure. Because of the large value of the specific surface area, we assumed that adsorption from the gas phase has a significant influence on the conductivity.

It is known that, H_2O molecules possess electron – donor properties under adsorption:

$$H_2O + S = H2O_{(ads)} + e^-$$

Adsorbed oxygen possess electron acceptor properties

$$½\ O2_{(g)} + V^{**}_o + 2e = O^*_o$$

We can explain the temperature dependence of the conductivity in the following way, changes in conductivity are related to the desorption and adsorption of water and oxygen molecules. Under heating, electron – donor H_2O molecules desorbed and the concentration of charge carriers decreased. In addition, the electron acceptor oxygen molecules occupying the adsorption sites of desorbed H_2O molecules. Molecular oxygen desorbs under heating more than H_2O molecules, Since ITO is oxygen deficit compound and oxygen molecules can become embedded in the crystal lattice.

CONCLUSION

The crystal structures of the samples were found to be a mixture of cubic and rhombohedra structures as determined from the XRD- analysis. The dielectric constant ε` of pure In_2O_3 is high compared with the samples containing different Tin ion concentrations which can be attributed to the change of crystal structure from cubic to a mixture of cubic and rhombohedra. The dielectric loss ε`` was found to be frequency dependent and ranged from 0.9 to 0.1. The ac-conductivity of the dielectric loss was calculated and found to be ranged from Log σ_{ac} = -9.839 (ohm^{-1} cm^{-1}) at room temperature to Log σ_{ac} = -4.162 (ohm^{-1} cm^{-1}) at 160 ^{0}C. The activation enthalpy and the entropy change of the prepared samples were calculated, it is found that the changes in the values are very low which make these materials good candidate to be used as substrate because of its independent on their constituents.

REFERENCES

Cho, Y-S., Gi-Ra Yi, Hong, JJ., Jang, SH. and Yang, SM. 2006. Colloidal Indium Tin Oxide nanoparticles for transparent and conductive films. Thin Solid Films. 515(4):1864- 1871.

El–Anwar, IM. and El-Sayed, AM. 1997. Some Electrical and Dielectric Properties of Titanium Substituted Li -Zn Ferrites. Egypt. J. Chem. 40 (4): 305-315.

Ellmer, K. and Mientus, R. 2008. Carrier transport in polycrystalline transparent conductive oxide: A comparative study of Zinc oxide and indium oxide. Thin solid films. 516 (14):4620-4627.

Jagadish, C., Ray, C., Saha, R. and Pramanik. 2003. Chemical Synethesis of Nanocrystalline Tin doped Cubic ZrO_2 Powders. Mater. Letts. 57(13-14): 2140-2144.

Kim, SS., Choi, SY., Park, CG. and Jin, HW. 1999. Transparent conductive ITO thin films through the sol – gel process using metal salts. Thin Solid Films. 347:155-160.

Korotcenkov, G., Nazarov, M., Zamoryanskaya, MV. and Ivanov, M. 2007. Cathod-luminescence emission study of nanocrystalline indium oxide films deposited by spray pyrolysis. Thin Solid Films. 515(20-21):8065-8071.

Lee, JS. and Choi, SC. 2005. Solvent effect on synthesis of indium tin oxide nanopowders by a solvothermal process. Journal of the European Ceramic Society. 25(14):3307-3314.

Malar, P., Mohanty, BC. and Kasiviswanathan, S. 2005. Growth and Rutherford backscattering spectrometry study of direct current sputtered indium oxide films. Thin Solid Films. 488 (1-2):26-33.

Pujilaksono, B., Klement, U., Nyborg, L., Jelvestam, U., Hill, S. and Burgard, D. 2005. X-ray Photoelectron Spectroscopy Studies of Indium Tin Oxide Nanocrystalline Powder. Materials Characterization. 54:1-7.

Rey, JFQ., Plivelic, TS., Rocha, RA., Tadokoro, RA., Torriani, I. and Muccillo, ENS. 2005. Synthesis of In_2O_3 Nanoparticles by Thermal Decomposition of a Citrate Gel Precursor. Journal of Nanoparticle Research. 7(2-3):203.

Richerson, DW. 1992. Modern Ceramic Engineering, Properties, Processing and Use in Design, Marcel Dekker, Inc. New York, Bassal, Hong Kong.

Sung, XW., Huang, HC. and Kwok, HS. 1996. On the initial growth of Indium Tin Oxide on Glass. Appl. Phys. Lett. 68:2663-2665.

Yang, H., Han, S., Wang, L., Kim, IlJ. and Son, YM. 1998. Preparation and Characterization of Indium-doped

tin dioxide Nanocrystalline powders. Materials Chemistry and Physics. 56:153.

Zhan, Z., Song, W. and Jiang, D. 2004. Preparation and property control of nanosized indium tin oxide particle. Journal of Colloid and Interface Science. 271, 366.

Zhu, H., Wang, N., Wang, L., Yao, K. and Shen, X. 2005. In Situ X-ray Diffraction Study of the Phase Transition of Nanocrystalline $In(OH)_3$ to In_2O_3. Inorganic Materials. 41 (6):609-612.

Received: Jan 23, 2009 Revised: May 16, 2009 Accepted: June 9, 2009